Journal of Genetics and Genomics 49 (2022) 934–942

Contents lists available at ScienceDirect

Journal of Genetics and Genomics

Journal homepage: www.journals.elsevier.com/journal-of-genetics-and-genomics/

Original research

Genetic evidence for facial variation being a composite phenotype of cranial variation and facial soft tissue thickness

Wei Qian [a, b, c, 1], Manfei Zhang [a, b, c, 1], Kaiwen Wan [d, 1], Yunxia Xie [e, 1], Siyuan Du [c], Jiarui Li [c], Xiongzheng Mu [f], Jiange Qiu [e], Xiangyang Xue [a, b, d], Xiahai Zhuang [d, *], Yingzhi Wu [f, *], Fan Liu [g, h, *], Sijia Wang [c, i, *]

[a] State Key Laboratory of Genetic Engineering, Human Phenome Institute, Zhangjiang Fudan International Innovation Center, Fudan University, Shanghai 201203, China
[b] School of Computer Science, Fudan University, Shanghai 200438, China
[c] CAS Key Laboratory of Computational Biology, Shanghai Institute of Nutrition and Health, University of Chinese Academy of Sciences, Chinese Academy of Sciences, Shanghai 200031, China
[d] School of Data Science, Fudan University, Shanghai 200433, China
[e] Academy of Medical Science, Zhengzhou University, Zhengzhou, Henan 450052, China
[f] Department of Plastic Surgery, Huashan Hospital, Fudan University, Shanghai 200040, China
[g] CAS Key Laboratory of Genomic and Precision Medicine, Beijing Institute of Genomics, University of Chinese Academy of Sciences, Beijing 100101, China
[h] School of Future Technology, University of Chinese Academy of Sciences, Beijing 101408, China
[i] Center for Excellence in Animal Evolution and Genetics, Chinese Academy of Sciences, Kunming, Yunnan 650223, China

ARTICLE INFO

Article history:
Received 16 September 2021
Received in revised form
17 February 2022
Accepted 20 February 2022
Available online 5 March 2022

Keywords:
Facial variation
Cranial variation
Association analysis
Single nucleotide polymorphism
Facial soft tissue thickness
Computed tomography

ABSTRACT

Facial and cranial variation represent a multidimensional set of highly correlated and heritable phenotypes. Little is known about the genetic basis explaining this correlation. We develop a software package ALoSFL for simultaneous localization of facial and cranial landmarks from head computed tomography (CT) images, apply it in the analysis of head CT images of 777 Han Chinese women, and obtain a set of phenotypes representing variation in face, skull and facial soft tissue thickness (FSTT). Association analysis of 301 single nucleotide polymorphisms (SNPs) from 191 distinct genomic loci previously associated with facial variation reveals an unexpected larger number of loci showing significant associations ($P < 1e{-}3$) with cranial phenotypes than expected under the null (O/E = 3.39), suggesting facial and cranial phenotypes share a substantial proportion of genetic components. Adding FSTT to a SNP-only model shows a large impact in explaining facial variance. A gene ontology analysis reveals that bone morphogenesis and osteoblast differentiation likely underlie our cranial-significant findings. Overall, this study simultaneously investigates the genetic effects on both facial and cranial variation of the same sample, supporting that facial variation is a composite phenotype of cranial variation and FSTT.

Introduction

A strong correlation exists between human facial and cranial morphology, likely due to sets of shared genetic components. Understanding the genetic basis explaining this correlation has guiding significance in human phenomics and genetic epidemiology, as well as has important implications in fields such as developmental biology, precision medicine, anthropology and forensic sciences.

Facial and cranial morphology each represents a set of highly correlated phenotypes, where strong correlations also exist between the two sets (Simpson and Henneberg, 2002; Albert et al., 2007; Duan et al., 2014; Kim and Shin, 2018). From genetic epidemiology perspective, it is reasonable to expect that cranial morphology is an endophenotype of facial morphology to a certain degree because a change of cranial shape is sufficient in resulting in a change of facial

* Corresponding authors.
E-mail addresses: zxh@fudan.edu.cn (X. Zhuang), wuyingzhi815@163.com (Y. Wu), liufan@big.ac.cn (F. Liu), wangsijia@picb.ac.cn (S. Wang).
[1] These authors contributed equally to this work.

https://doi.org/10.1016/j.jgg.2022.02.020

shape but not vice versa. On the other hand, facial morphology may be considered a composite phenotype composed of skull and soft-tissue variation. Given the high heritability of both facial and skull morphology (Liu et al., 2012; Weinberg et al., 2013; Seselj et al., 2015; Cole et al., 2017; Tsagkrasoulis et al., 2017), they serve as perfect reference traits to elucidate the relationships between endo and composite phenotypes.

Over the last years, a significant progress in understanding the genetic basis of facial variation has been made by a series of well-sized genome-wide association studies (GWASs). These studies typically apply advanced image processing technologies to quantify facial phenotypes from 2D or 3D facial photos, and screen for face-associated DNA variants over the genome in a variety of population samples. To date, a total of about 365 candidate single nucleotide polymorphisms (SNPs) at 235 distinct genomic loci have been identified for association with the facial variation at the genome-wide significance level (Liu et al., 2012; Paternoster et al., 2012; Adhikari et al., 2016; Cole et al., 2016; Pickrell et al., 2016; Shaffer et al., 2016; Lee et al., 2017; Cha et al., 2018; Claes et al., 2018; Crouch et al., 2018; Qiao et al., 2018; Li et al., 2019; Xiong et al., 2019; Huang et al., 2020; Bonfante et al., 2021; White et al., 2021). The allelic effects at the associated loci were typically small, together explaining on average 5%−10% of the phenotypic variance (Claes et al., 2014; Lippert et al., 2017; Qiao et al., 2018; Xiong et al., 2019), confirming a highly polygenic nature of facial variation. A substantial proportion of the associated SNPs also demonstrated a multi-trait effect with various allele effect sizes, thus providing a genetic explanation for the correlations between different facial phenotypes. Most of the robust associations concentrate on the central part of the face (eye, nose, jaw) where the thickness of the soft-tissue seems having less variance (Stephan and Simpson, 2008; Baillie et al., 2016). While the genetic progress on facial variation are significant, genetic studies on the cranial counterpart are scarce, likely due to the difficulties in obtaining sufficient skull samples. Forensic studies aiming to reconstruct facial shape from a skull for individual identification purposes have described extensively the characteristics of facial soft tissue thickness (FSTT) and its large influence on the accuracy of facial reconstruction (De Greef et al., 2006; Simmons-Ehrhardt et al., 2018). However, few studies have ever explored facial variation composed of skull variation and FSTT in the context of genetics.

In this study, we investigated the genetic basis explaining the relationships between facial (composite phenotype) and cranial morphology (endophenotype) by examining how candidate SNPs previously reported in facial GWASs may influence cranial morphology. We obtained 125 facial phenotypes, 125 cranial phenotypes and 35 FSTT phenotypes in 777 Han Chinese women using advanced image analysis of head CT scans. We tested the association between a set of 301 previously identified face-associated SNPs and facial, cranial and FSTT phenotypes. Our results revealed the genetic architecture underlying the correlation of facial and cranial variation, supporting that facial morphology is a composite phenotype with cranial morphology and soft tissue thickness as key components.

Results

Automated landmarking of skull and face landmarks (ALoSFL)

This study was conducted in a relatively young female cohort (mean age = 26.01 ± 5.04) of Han Chinese origin (Fig. S1) with a narrow variation in body mass index (BMI, mean = 19.34 ± 2.02, Table S1). We focused on 15 anatomical facial landmarks which also have corresponding landmarks on their cranial counterpart (Fig. 1A and 1B; Table S2; Materials and methods). We developed a novel software package, Automated Landmarking of Skull and Face Landmarks (ALoSFL), to simultaneously locate facial and cranial landmarks from head CT images (Figs. 1C and S2; Materials and methods). In a testing set of 20 samples, intra-rater, inter-rater and ALoSFL correlations were all very high for both facial and cranial landmarks ($r > 0.98$; Table S3). ALoSFL errors were fairly close to inter-rater differences (face: 2.43 mm, skull: 2.15 mm; Fig. S3). For bilateral zygomatic points, larger variations were observed for intra-rater differences (1.61 mm−1.75 mm), inter-rater differences (2.54 mm−3.23 mm), and ALoSFL errors (3.70 mm−4.76 mm; Table S3). This is likely explained by the fact that bilateral zygomatic points are more difficult to be located precisely. These results evidently support the reliability of ALoSFL in simultaneously locating facial and cranial landmarks from head CT images.

Face-associated SNPs affect cranial morphology

We investigated 125 phenotypes for facial and cranial variation and 35 phenotypes for FSTT, including Euclidean distances between landmarks (105 pairwise inter-landmark distances for facial and cranial variation, 15 intra-landmark distances for FSTT) and top 20 principal components (PCs) from a shape analysis (Fig. S4; Materials and methods). The distributions of FSTT observed in our data were in high consistency with anatomical knowledge (Fig. S5). Age and BMI showed significant effects on facial and cranial phenotypes, and their explained variances of facial phenotypes were on average greater than that of cranial phenotypes as expected (Fig. S6; Table S4).

Considering inter-landmark distances, strong correlations were observed between cranial and facial phenotypes (Pearson's correlation $r = 0.84 \pm 0.07$), among which the highest correlations were concentrated in the central area of the face/skull, mainly involving the surface points of the inner and outer corners of the eyes, nose and mandible. The relatively lower correlations mainly scattered to the sides of the face/skull, involving the zygoma, nasal alar, and lip (Fig. S7), which are characterized by less accurate anatomical definitions or relatively thicker soft tissue. These results suggest that facial and cranial phenotypes generally harbor substantially high correlations.

The genetic association analysis included 301 candidate SNPs from 191 distinct genomic loci (Table S5). Overall, the association *P*-values for facial and cranial phenotypes significantly deviated from the null distribution that was obtained based on permutations from genome background SNPs (Kolmogorov-Smirnov test, $P = 4.98e{-4}$ for face and $P = 4.06e{-4}$ for skull; Fig. 2A). The association *P*-values for FSTT phenotypes also nominally significantly deviated from the null but at a much lower level of significance ($P = 0.03$; Fig. S8). These results confirm that the set of candidate SNPs overall has a genuine effect on facial and cranial variation.

The association analyses were conducted under different thresholds (1e−2, 1e−3, 1e−4, 1e−5; Table 1). The threshold of 1e−5 roughly corresponds to our study-wide type-I error of 0.05 after adjusting for multiple testing (Materials and methods). Under this threshold (1e−5), our data however did not have power to detect any significant association. Because our study does not aim to identify new associations but rather to investigate the effects of a set of well-established face-associated SNPs, we report our results under a relaxed threshold of 1e−3. Under this relaxed threshold, the power of our sample for detecting an additive allele at the frequency of 0.2 with a standardized effect size of 0.2 was about 50% (Materials and methods). Among the 191 previously established face-associated loci, 34 showed significant ($P < 1e{-3}$) associations

A

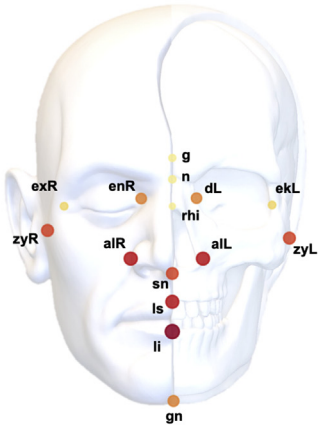

B

ID	Facial landmarks	Cranial landmarks
1	Glabella (g)	Glabella (g)
2	Nasion (n)	Nasion (n)
3	Nose bridge (rhi)	Rhinion (rhi)
4	Left alare (alL)	Left alare (alL)
5	Right alare (alR)	Right alare (alR)
6	Subnasale (sn)	Nasospinale (ns)
7	Left entocanthion (enL)	Left dacryon (dL)
8	Right entocanthion (enR)	Right dacryon (dR)
9	Left ectocanthion (exL)	Left ektoconchion (ekL)
10	Right ectocanthion (exR)	Right ektoconchion (ekR)
11	Left zygion (zyL)	Left zygion (zyL)
12	Right zygion (zyR)	Right zygion (zyR)
13	Labrale superius (ls)	Prosthion (pr)
14	Labrale inferius (li)	Infradentale anterius (id)
15	Gnathion (gn)	Gnathion (gn)

C

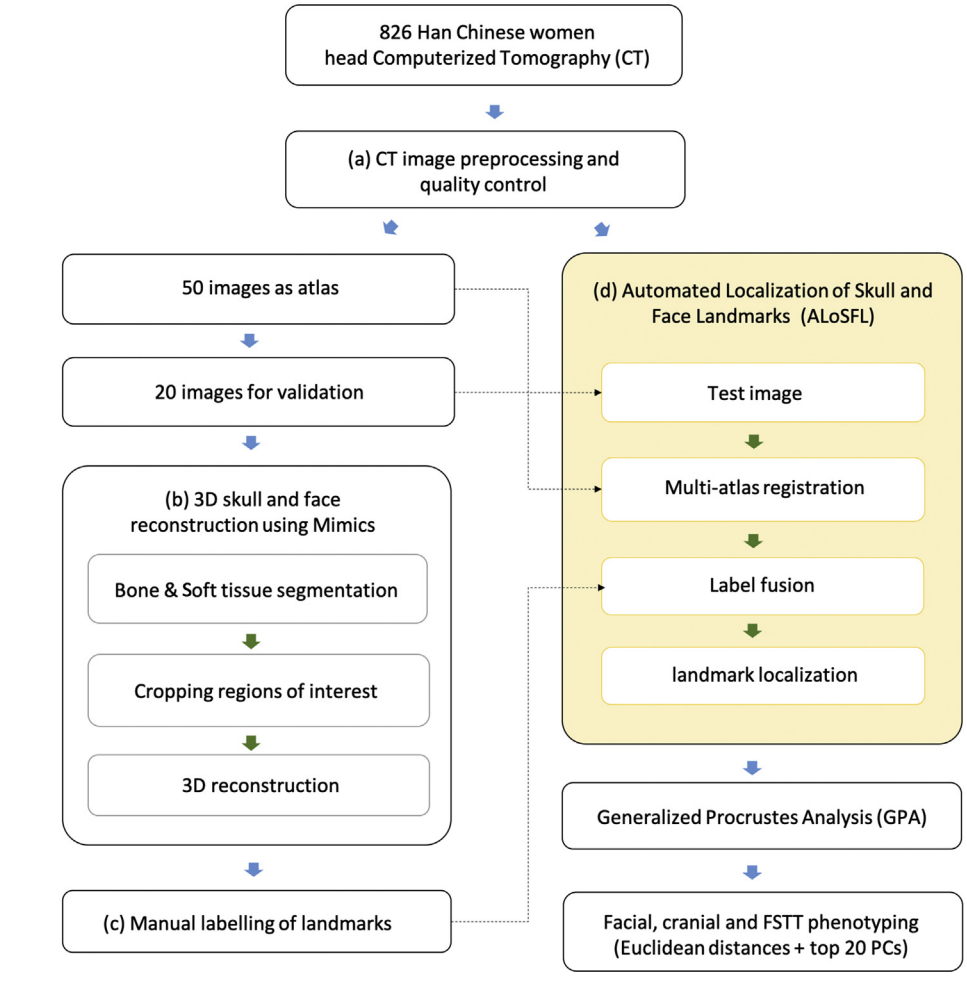

Fig. 1. Automated localization of facial and cranial landmarks from head CT images. **A**: A reference face and skull illustrates the 15 facial and cranial landmarks with the FSTT of each landmark proportional to the redness and the node size. **B**: The names of the 15 facial and the corresponding cranial landmarks. **C**: The overall flowchart of ALoSFL for automated localizing facial and cranial landmarks.

with facial, cranial, or FSTT phenotypes (Fig. 2B; Table S6). Among the 34 highlighted loci, 20 were associated with distance-based phenotypes, 19 were associated with shape PCs with 5 overlapping with distance-associated loci (Fig. 2D). The 14 PC-only significant loci were generally weakly ($1e{-}3 < P < 0.05$) associated with multiple distance phenotypes, confirming a presence of multi-trait effects of the genetic variants. Among the 34 highlighted loci, 18 were associated with facial phenotypes, 22 were associated with cranial phenotypes with 12 overlapping with the face-associated loci, and 9 were associated with FSTT phenotypes with 3 overlapping with the face- or skull-associated loci (Fig. 2C; Table 1). The ratio of the number of observed signals over the expected number under the null was large for cranial phenotypes (O/E = 3.39) and facial phenotypes (O/E = 2.77) but smaller for FSTT phenotypes (O/

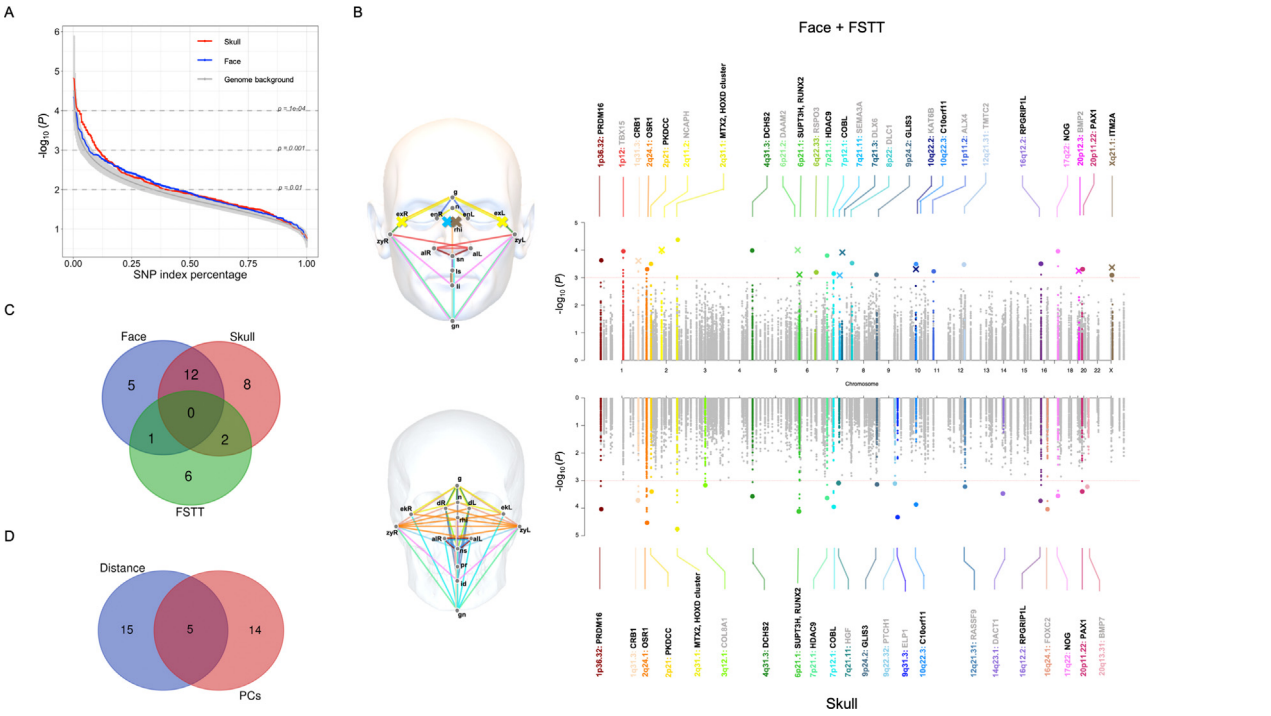

Fig. 2. SNPs associated with facial, cranial and FSTT phenotypes in 777 Han Chinese women. **A**: *P*-value quantiles for association between 301 previously established face-associated SNPs and 125 facial (blue curve) and cranial (red curve) phenotypes. The genome background *P*-value quantiles were obtained by randomly resampling 301 SNPs for 1000 replicates, where the dark gray curve denotes the mean values of the 1000 replicates and the light gray area represents the 95% interval of the 1000 replicates. **B**: The right panel displays the association results for the 301 SNPs and 125 facial phenotypes (dots in the upper part), 35 FSTT phenotypes (crosses in the upper part), and 125 cranial phenotypes (dots in the lower part). The $-\log_{10}$(*P*-values) for all SNPs were plotted against the chromosomal positions. The dotted red line corresponds to the threshold of $P = 1e{-}3$. The lead SNPs in distinct genomic loci are highlighted in different colors. The candidate genes reported in previous GWASs in these loci are denoted in text, where bold font indicates significant for at least two types of phenotypes (facial, cranial, and FSTT). The significant associations with inter-landmark distances (lines) and FSTT (crosses) are superimposed on face/skull maps (the left panel), with the same color scheme as the right panel. **C**: A Venn diagram for the number of distinct loci associated with facial, cranial and FSTT phenotypes. **D**: A Venn diagram for the number of distinct loci associated with inter-landmark distances and shape PCs.

Table 1
The number of associations under different thresholds.

Threshold	N_SNPs	Face and skull (N_phenotypes 34)					FSTT (N_phenotypes 26)		
		E	Face	(O/E)	Skull	(O/E)	E	FSTT	(O/E)
1e−2	191	64.94	96	1.48	91	1.40	49.66	61	1.23
1e−3	191	6.49	18	2.77	22	3.39	4.97	9	1.81
1e−4	191	0.65	2	3.08	4	6.16	0.50	0	0.00
1e−5	191	0.06	0	0.00	0	0.00	0.05	0	0.00

Note: N_SNPs, the number of independent tests after removing linkage disequilibrium; N_phenotypes, the number of independent tests after adjusting for phenotype correlations; E, the expected number under the null; O/E, the ratio of observed number and expected number under the null; Face, the number of SNPs associated with facial phenotypes under the threshold. Skull, the number of SNPs associated with cranial phenotypes under the threshold; FSTT, the number of SNPs associated with FSTT phenotypes under the threshold. The threshold of 1e−5 corresponds to 5% study-wide type-I error after fully adjusting for all independent tests.

E = 1.81; Table 1). This strongly suggests that facial and cranial variation share a substantial proportion of genetic components but less conclusive for FSTT. We therefore focus more on facial and cranial associations in our follow-up analyses.

Interestingly, the association signals that were more significant for cranial phenotypes than facial phenotypes more likely involve landmarks of thinner FSTT such as the eyes, nasal frontal area and the nasion (Fig. 3A–3C), while those signals more significant for facial phenotypes than cranial phenotypes more likely involve landmarks of thicker FSTT such as the lip, the nose wings and the cheeks (Figs. 3D and S9). These observations may be explained by their biological functions. For example, mutations in *OSR1* were found to cause abnormal skeleton morphology in mice (Bult et al., 2019). *HOXD* genes were reported to regulate limb development and skeletal patterning (Zakany et al., 2004). Loss of *MTX2* leads to mandibuloacral dysplasia (Elouej et al., 2020). Furthermore, repeating the association analysis by including the FSTT as covariates identified one additional locus showing significant association with facial phenotype, i.e., rs6568401 near *PRDM1* on chromosome 6q21 was associated with the distance between the upper and lower lips (before adjustment, $P = 1.06e{-}3$; after adjustment, $P = 9.42e{-}5$; Table S6), confirming a gain of power in the analysis of the facial phenotypes with large variation in FSTT.

Differential biological processes between cranial and facial morphogenesis

We carried out a gene ontology (GO) analysis to compare a set of skull-associated genes ($n = 34$) with a set of face-associated genes ($n = 28$; Materials and methods). Overall, skull-associated genes harbored a larger number of significantly enriched GO terms than face-associated genes (Fig. S10A). For the GO terms shared between the two gene sets, skull-associated genes were generally more significant than face-associated genes. These included "embryonic morphogenesis" ($P_{skull} = 1.00e{-}20$, $P_{face} = 1.00e{-}16$), "skeletal system development" ($P_{skull} = 1.00e{-}18$, $P_{face} = 1.00e{-}17$), "cartilage development" ($P_{skull} = 6.31e{-}8$, $P_{face} = 2.51e{-}5$), "pattern specification process" ($P_{skull} = 1.00e{-}20$, $P_{face} = 1.00e{-}17$) and "ossification" ($P_{skull} = 1.26e{-}8$, $P_{face} = 6.31e{-}3$). The skull-unique terms were "bone morphogenic protein (BMP) signaling pathway" ($P_{skull} = 6.31e{-}4$), "positive

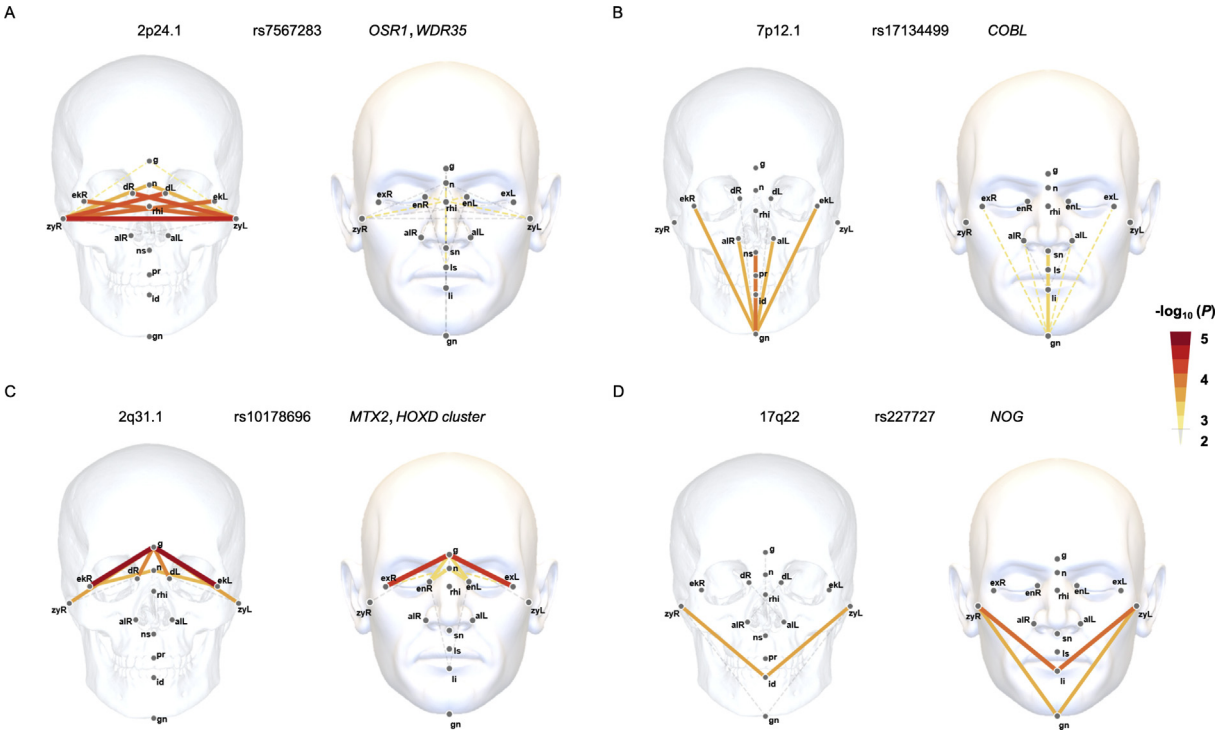

Fig. 3. Examples of genetic effects on face and skull. **A**: rs7567283 near *OSR1-WDR35*. **B**: rs17134499 near *COBL*. **C**: rs10178696 near *MTX2* and *HOXD* cluster. **D**: rs227727 near *NOG*. The association *P*-values are plotted at the −log10 scale on a reference face and skull to illustrate the genetic effects on facial and cranial variation. The association significance is proportional to the redness and the width of the lines. Solid lines denote $P < 1e{-}3$ and dashed lines denote $1e{-}3 < P < 1e{-}2$.

regulation of bone mineralization" ($P_{skull} = 1.26e{-}5$) and "regulation of osteoblast differentiation" ($P_{skull} = 3.98e{-}7$), whereas face-unique terms included "roof of mouth development" ($P_{face} = 6.31e{-}5$)" and "forebrain development" ($P_{face} = 5.01e{-}3$; Fig. S10A; Table S8). A network analysis of protein–protein interactions among the skull- and face-associated genes identified a subnetwork of 27 interacting proteins, including *BMP7*, *TBX15* and *HOXD13* with much higher network degree representing the three clusters of genes associated either with skull, or face or both (Fig. S10B; Materials and methods). These results indicate that bone morphogenesis related pathways may explain the different gene sets in association with facial and cranial phenotypes.

Facial variation as a composite phenotype of cranial variation and FSTT

We obtained several lines of evidence supporting that facial variation is a composite phenotype of cranial variation and FSTT. First, FSTT was positively correlated with almost all facial landmarks (mean $r1 = 0.20$), cranial landmarks were highly positively correlated with facial landmarks (mean $r2 = 0.79$), but the correlations between FSTT and cranial landmarks were on average much weaker (mean $r3 = -0.02$; Figs. 4A, 4B, S11). The derivation of various correlations are detailed in the Materials and methods section. Second, the correlation between a pair of corresponding facial and cranial landmarks is different for different landmarks depending on the FSTT of that landmark, i.e., thicker soft tissue led to a reduced correlation between a pair of corresponding facial and cranial landmarks (Pearson's correlation $r4 = -0.60$, $P = 0.02$; Fig. 4C). Third, the genetic effect on the skull was positively correlated with the facial–cranial correlations (Pearson's correlation $r = 0.21$; $P = 0.03$) but the genetic effect on the face did not show any statistically significant correlation with the facial–cranial correlations ($P = 0.30$; Fig. 4D). These findings generally support the hypothesis that facial variation is a composite phenotype of cranial variation and FSTT. It also should be noted that these observations were based on a relatively small sample, which requires further validation by experimental design in future studies.

A correlation partitioning analysis was carried out to investigate the contribution of a set of 20 SNPs and FSTT in explaining the facial–cranial correlations based on a previously proposed *C* statistic (Chen et al., 2021). These 20 SNPs were significantly associated with facial or cranial phenotypes in terms of inter-landmark distances (Table S6). The analysis showed that SNPs and FSTT together explained on average 4.08% facial–cranial correlations, significantly much higher than the SNPs alone (1.91%, Wilcoxon signed-rank test $P = 1.04e{-}11$; Fig. 4E and 4F). The top explained facial–cranial correlation was the distance between glabella and nasion (g–n), for which the SNPs and FSTT together explained 13.24% and the SNPs alone explained 0.69%. The top facial–cranial correlation explained by the SNPs alone was 5.06% for g-zyL/R phenotypes where adding the effect of FSTT could explain 6.86% (Table S9). These results confirm the genetic variants and FSTT together explain the correlation between cranial and facial morphology.

A prediction analysis was carried out to compare different models in predicting facial phenotypes (Materials and methods). This analysis demonstrates that the genetic model fitted for predicting cranial phenotypes (model 3 in Fig. 4H) could explain a similar proportion of facial variance compared with the model fitted for predicting facial phenotypes (model 1 in Fig. 4H), and adding FSTT could substantially enhance the explainable facial variance (models 2 and 4 in Fig. 4H). More specifically, the SNP-only model fitted for predicting facial phenotypes (model 1) explained on average 1.78% and up to 4.94% (gn-exL/R) facial variance. Adding FSTT variables (model 2) explained a significantly higher proportion of facial variance (mean $R^2 = 4.91\%$, up to 14.16% for zyL-zyR). Cranial phenotypes predicted using the SNPs (model 3) explained on average 1.71% and up to 4.66% (gn-exL/R) facial variance

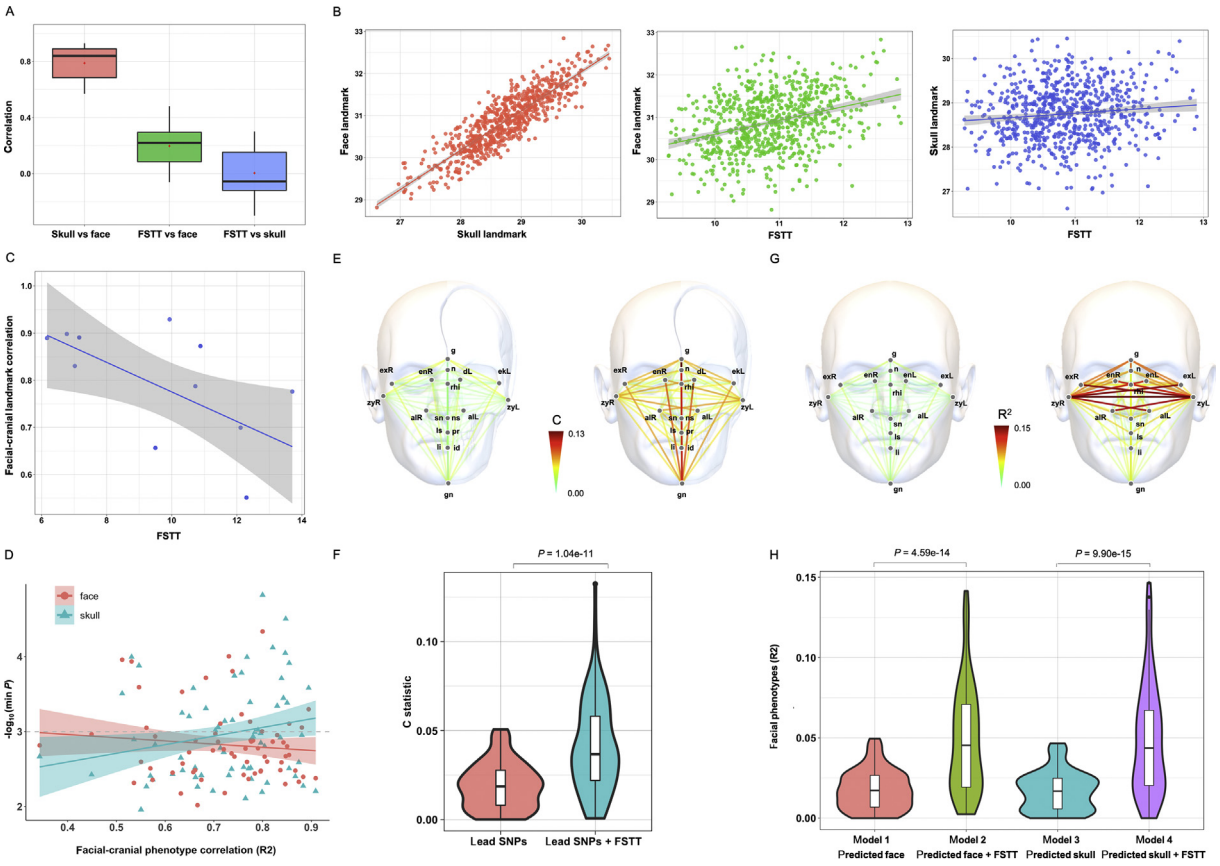

Fig. 4. Facial variation is a composite phenotype of skull variation and FSTT. **A**: Boxplots showing high correlation between cranial landmarks and facial landmarks (red), positive correlation between FSTT and almost all facial landmarks (green), but much weaker correlation observed between FSTT and cranial landmarks on average (blue). **B**: The example of zy landmark illustration. **C**: A negative correlation between the average FSTT of each landmark and facial–cranial landmark correlations (see Materials and methods). **D**: Correlations between facial–cranial phenotypic correlation and the association *P*-values considering 301 face-associated SNPs and 105 pairwise inter-landmark distance phenotypes. For each phenotype, minimum *P*-value across the SNPs is plotted. Cranial phenotypes (blue triangles) show positive correlations, but facial phenotypes (red dots) are statistically uncorrelated. **E** and **F**: A correlation partitioning analysis investigates the contribution (*C* statistic) of the selected 20 lead SNPs and FSTT in explaining the facial–cranial correlations. Boxplots show that the 20 lead SNPs and FSTT together (the right reference face/skull) explain significantly higher proportions of facial–cranial correlations than the lead SNPs alone (the left reference face/skull). **G** and **H**: A LOOCV based prediction analysis using multivariate linear regression models evaluates the facial variance explained by the predicted face/skull based on the 20 lead SNPs and FSTT. Boxplots show the proportions of facial variance explained by predicted face (model 1), predicted face combined with FSTT (model 2), predicted skull (model 3) and predicted skull combined with FSTT (model 4). The left reference face illustrates facial variance explained by a predicted skull alone (model 3) and adding FSTT as an additional predictor (model 4) substantially enhance the explainable facial variance on the right reference face.

(Fig. 4G). Adding the FSTT variables (model 4) significantly enhanced the explainable variance (mean R^2 = 4.90%, up to 14.65% for zyL-zyR; Fig. 4G; Table S10). These results support facial variation is a composite phenotype of cranial variation and FSTT.

Discussion

This study simultaneously investigated the genetic association of facial and cranial phenotypes obtained in the same sample. We developed ALoSFL for localizing both facial and cranial landmarks from head CT images in a fully automated manner. We identified that previously established face-associated SNPs also showed significant effects on cranial variation, often with even larger effects than their effects on facial variation. Functional enrichment analyses further provided evidence for differential biological processes between the cranial and facial significant gene sets. A model fitting analysis confirmed that genetic factors and FSTT independently explain a substantial proportion of facial variation, supporting our hypothesis that facial variation is a composite phenotype of cranial variation and FSTT. These findings are of guiding importance for genetic studies of human complex traits.

Our genetic association analysis revealed that cranial variation and FSTT are potential endophenotypes of facial variation. Endophenotype, a key concept in genetic epidemiology, is a term used to separate a composite phenotype into more stable phenotypes with stronger genetic connections (Gottesman and Gould, 2003; Preston and Weinberger, 2005). As suggested by our study, GWASs separately conducted for cranial variation and FSTT are expected to deliver extended lists of genetic variants that are more directly associated with the endophenotypes, thus boosting the explained variance of facial variation. In addition, adjusting for FSTT in facial GWASs may increase the statistical power in detecting effect alleles. In modern molecular epidemiology, the concept of endophenotype is further extended by considering different layers, such as genetic variations and epigenetic modifications (Miller and Rockstroh, 2016). Understanding the complex interactions between and within the layers is critical for explaining the heritability of the composite phenotype (Greenwood et al., 2019). Future studies focusing on integrated analyses of multi-omics datasets may further enhance our understanding of the genetic architecture of human facial variation.

With ALoSFL, 50 labeled atlas images are sufficient to achieve a similar accuracy level to a recent deep learning-based approach using more training samples (Yun et al., 2020), but the accuracy

largely depends on the choice of landmarks, that is, more anatomically precisely defined, more accurate, in line with previous findings (Montufar et al., 2018; Yun et al., 2020). Importantly, ALoSFL facilitates FSTT estimation from simultaneous cranial and facial landmarking, which is highly consistent with the FSTT measurements obtained from manual point placement (Hwang et al., 2015) and the dense map of facial tissue depths manually built from CT images (Simmons-Ehrhardt et al., 2018).

Thirteen of our confirmed 34 loci have been repeatedly associated with facial variation in multiple independent GWASs (Liu et al., 2012; Adhikari et al., 2016; Cole et al., 2016; Pickrell et al., 2016; Cha et al., 2018; Claes et al., 2018; Xiong et al., 2019; White et al., 2021), with more cranial-significant loci than facial-significant loci (Table S6). Further evidence from existing literature supports that our cranial-significant genes play a critical role in bone morphogenesis and osteoblast differentiation during craniofacial development (Calloni et al., 2009; Chen et al., 2020).

Regarding the limitations of the study, our estimation of FSTT might be influenced by the difference between upright and supine positions due to gravitational shift (Bulut et al., 2017). Nonetheless, our landmark-based phenotyping in a relatively young female cohort with lower variation in BMI should be less affected. The relatively small sample size as indicated by our power analysis, which may lead to false negative results, although our study does not intend to discover new loci. Despite of the limited sample size, we observed an unexpected large number of genetic associations at relaxed significance thresholds for both facial and cranial phenotypes.

In conclusion, our findings strongly pinpoint the significance of genetic study on cranial variation and we have provided a pioneer example for elucidating the genetic basis explaining the correlation between the composite and the endophenotype. It is reasonable to expect that large-scale GWASs of cranial variation and FSTT will provide a more comprehensive figure of the complex genetic architecture shared between facial and cranial variation.

Materials and methods

Samples

A total of 826 unrelated Han Chinese women voluntarily participated in this study via the department of plastic surgery, Huashan Hospital affiliated to Fudan University, Shanghai, China from 2019 to 2021. This study was approved by Ethics Committee of Huashan Hospital affiliated to Fudan University, Shanghai, China (Registration number 2021-150). All volunteers provided written informed consent. This study is compliant with the Guidance of the Ministry of Science and Technology (MOST) for the Review and Approval of Human Genetic Resources. All volunteers underwent micro plastic surgery for cosmetic purpose. Head CT images were collected before surgeries, thus not affecting the genetic association. The inclusion criteria include (1) no craniofacial morphology; (2) no head injury; (3) no craniofacial disease, thyroid disease, pituitary disease, or tumors; and (4) no medical conditions that affect growth and development. After all phenotypic and genotypic quality controls (see below), this study included a total of 777 women.

CT image preprocessing, 3D reconstruction and manual landmarking

Whole head CT scans were performed on SIEMENS spiral CT scanner with 20–466 in slice number, 0.6–1 mm in slice thickness and 512 × 512 μm in resolution. Raw images in DICOM format with slice number < 50 or with metal objects were removed. 3D reconstruction and manual landmarking were performed using Mimics v15.0 (Materialise; Leuven, Belgium), including (1) segmentation of bone and soft tissues using the default Hounsfield unit thresholds respectively, (2) cropping and trimming to remove the neck, hair and imaging artifacts, and (3) Frankfurt Horizontal plane transformation. We focused on 15 pairs of landmarks having correspondences between the face and the skull (Table S2). These landmarks, mainly located in the midface, are anatomically well defined with relatively high heritability estimates (Wu et al., 2019; Xiong et al., 2019), and have been repeatedly used in previous GWASs of facial variation. To access inter-rater concordance, two experienced clinicians manually labeled the 15 landmarks. For intra-rater comparison, one clinician repeated the labeling after two weeks. All images were resampled to 2 × 2 × 2 mm for subsequent analyses.

Automated localization of skull and face landmarks (ALoSFL)

ALoSFL was developed based on multi-atlas registration and label fusion algorithms (Zhuang et al., 2011). The training and testing sets consisted of 50 and 20 labeled images as atlas (reference) and validation respectively, and both were randomly selected from all samples. The atlas images with manual labels were considered as targets. Test images were registered to match each of the targets through spatial transformation using both linear and nonlinear deformation. Deformation of test images was conducted by maximizing mutual information. The predicted landmarks proposed by the top five atlas images most similar to the test image were fused into the final positionings of landmarks by averaging. For each landmark, the average coordinate of intra-rater labeling was considered as the reference. Euclidean distances were computed between ALoSFL and the reference and compared with the inter-rater difference. ALoSFL was applied to the full dataset to obtain facial and cranial landmarks. All landmarks were visually checked and manually fine-tuned using Mimics. Generalized Procrustes analysis (GPA) was conducted to remove affine variations due to shifting, rotation and scaling.

Facial, cranial, and FSTT phenotypes

FSTT values were calculated as the Euclidean distances between the facial and the corresponding cranial landmarks, and therefore 15 FSTT phenotypes were obtained. For symmetrical landmarks (zy, ex, en, al), average values were used. A total of 105 inter-landmark Euclidean distances were derived for both the face and the skull. For symmetric phenotypes, average values of the left and right sides were used. The vast majority of our phenotypes followed the normal distribution (adjusted $P > 0.05$, Shapiro–Wilk test). Outliers with more than three standard deviations were removed and Z-normalized phenotypes were used in the subsequent analyses. Landmark PCs were derived using R package shapes v1.2.6 (Dryden and Mardia, 2016). The top 20 PCs were selected as PC phenotypes. Therefore, this study included a total of 125 facial phenotypes, 125 cranial phenotypes and 35 FSTT phenotypes.

DNA genotyping, quality control and imputation

DNA samples were genotyped on Illumina Infinium Global Screening Array 650K. Samples with incorrect gender, missing rate > 5%, |heterozygosity| > 0.2, duplicates and second-degree relatives were excluded. SNPs with minor allele frequency (MAF) < 1%, call-rate < 97%, Hardy–Weinberg P-value < 1e–5, and samples missing > 2% were excluded. Pre-phasing was performed in SHAPEIT2 (Delaneau et al., 2011), and imputation was performed using IMPUTE2 (Howie et al., 2009) based on the 1000 Genome Project (GP) Phase 3 reference panel (Genomes Project et al., 2015). After post-imputation quality control, 7,551,003 SNPs were obtained.

Genomic principal component analysis was conducted to confirm that all our samples are of East Asian ancestry using the 1000GP datasets.

Statistical analyses

Out of the 365 SNPs previously reported in facial GWASs (Table S5), 301 were included after quality control. Genetic association was tested using PLINK v2.0 (www.cog-genomics.org/plink/2.0/) by linear regression under an additive genetic model, with age, BMI and the first 10 genomic PCs as covariates. Bonferroni correction was used to adjust the effective number of independent variables, which was estimated using the matrix spectral decomposition method (Li and Ji, 2005). The threshold for fully adjusting for multiple tests was roughly 1e−5 with 34 independent phenotypes for face and skull and 26 independent phenotypes for FSTT and 191 independent loci. The association analyses were conducted under different thresholds (1e−2, 1e−3, 1e−4, 1e−5). A power analysis was performed by simulating data based on an additive genetic model at the effect allele frequency of 0.2 with standardized effect size of 0.2 under the sample size of 800 and various conditions of statistical significance threshold alpha. Permutation tests were conducted by randomly selecting 301 SNPs from the genome background and repeating for 1000 times. Genetic association of the random sets of SNPs were tested with facial, cranial, and FSTT phenotypes, respectively. For each iteration, the minimum *P*-value of each SNP across phenotypes was used. Kolmogorov–Smirnov (KS) test (Massey, 1951) was used to compare the distribution of *P*-values between random SNPs from the genome background and 301 face-associated candidate SNPs for facial, cranial and FSTT phenotypes respectively.

Considering facial landmark data F as an n by m matrix consisting of n individuals and m landmarks, the distance from a facial landmark j to the origin is calculated based on landmark coordinates, denoted as F_j, so are S for cranial landmark data and T for FSTT with the same dimension. The correlations between a facial landmark, the corresponding cranial landmark and its FSTT are derived as $r1_j = cor(F_j, T_j)$, $r2_j = cor(F_j, S_j)$ and $r3_j = cor(S_j, T_j)$ respectively. $r4 = cor(\overline{T}, r1)$ denotes the correlation between the average FSTT and the facial–cranial correlation across landmarks.

A correlation partitioning analysis was conducted using a C statistic (Chen et al., 2021). For each facial phenotype, a prediction analysis based on leave-one-out cross validation (LOOCV) was carried out to assess the predictabilities of four models. Model 1 only included the 20 lead SNPs, model 2 additionally included FSTT variables of the two landmarks for an inter-landmark phenotype, model 3 included a predicted cranial phenotype using the 20 SNPs, model 4 included FSTT variables in addition to the predicted cranial phenotype. The predicted face/skull was obtained by fitting a multivariate linear regression model.

A gene ontology enrichment analysis was carried out using Metascape (Zhou et al., 2019). Gene ontology terms were classified into four categories: a) morphogenesis, b) development, c) differentiation and d) signaling and regulation (Table S8). A total of 41 face- and skull-associated genes were included, which are either physically closest to the regional SNPs or have been reported in previous studies (Table S5). A protein–protein interaction (PPI) network analysis was applied using STRING database (Szklarczyk et al., 2019), with a subnetwork of connected candidate genes. The subnetwork was analyzed and clustered by Cytoscape using Markov Cluster algorithm (Shannon et al., 2003).

Statistical analyses were performed using R v4.0.3 and Python v3.7.4 unless otherwise specified.

Data availability

Summary statistics are available on the National Omics Data Encyclopedia (NODE) (https://www.biosino.org/node/project/detail/OEP002650), with project ID OEP002650. Data usage shall be in full compliance with the Regulations on Management of Human Genetic Resources in China. ALoSFL software is freely available on GitHub (https://github.com/kevinwolcano/ALoSFL).

CRediT authorship contribution statement

Wei Qian, **Manfei Zhang**: Conceptualization, Formal analysis, Methodology, Data curation, Investigation, Validation, Visualization, Writing - Original draft, Review & Editing. **Kaiwen Wan**, **Yunxia Xie**: Methodology, Validation, Formal analysis, Writing - Original draft, Review & Editing. **Siyuan Du**, **Jiarui Li**: Visualization, Writing - Review & Editing. **Xiongzheng Mu**: Resources, Supervision. **Jiange Qiu**: Investigation, Validation. **Xiangyang Xue**: Funding acquisition, Supervision. **Xiahai Zhuang**: Methodology, Supervision, Writing - Review & Editing. **Yingzhi Wu**: Resources, Data curation, Supervision, Writing - Review & Editing. **Fan Liu**: Funding acquisition, Supervision, Writing - Original draft, Review & Editing. **Sijia Wang**: Conceptualization, Funding acquisition, Project administration, Supervision, Writing - Review & Editing.

Conflict of interest

The authors declare that they have no conflicts of interest regarding this work.

Acknowledgments

We thank for all suggestions collected during the poster exhibition of the Society for Craniofacial Genetics and Developmental Biology (SCGDB) 2019 Annual Meeting. We thank all the participants in these studies. This project was supported by the following grants and contracts: Strategic Priority Research Program of Chinese Academy of Sciences (XDB38020400, XDB38010400, XDC01000000); Shanghai Municipal Science and Technology Major Project (2017SHZDZX01, 2018SHZDZX01); National Key Research and Development Project (2018YFC0910403); CAS Interdisciplinary Innovation Team Project; Max Planck-CAS Paul Gerson Unna Independent Research Group Leadership Award; Science and Technology National Natural Science Foundation of China (31900408, 81930056); China Postdoctoral Science Foundation (2019M651352, 2020M670984). Service Network Initiative of Chinese Academy of Sciences (KFJ-STS-ZDTP-079).

Supplementary data

Supplementary data to this article can be found online at https://doi.org/10.1016/j.jgg.2022.02.020.

References

Adhikari, K., Fuentes-Guajardo, M., Quinto-Sanchez, M., Mendoza-Revilla, J., Camilo Chacon-Duque, J., Acuna-Alonzo, V., Jaramillo, C., Arias, W., Lozano, R.B., Perez, G.M., et al., 2016. A genome-wide association scan implicates DCHS2, RUNX2, GLI3, PAX1 and EDAR in human facial variation. Nat. Commun. 7, 11616.

Albert, A.M., Ricanek, K., Patterson, E., 2007. A review of the literature on the aging adult skull and face: implications for forensic science research and applications. Forensic Sci. Int. 172, 1–9.

Baillie, L.J., Muirhead, J.C., Blyth, P., Niven, B.E., Dias, G.J., 2016. Position effect on facial soft tissue depths: a sonographic investigation. J. Forensic Sci. 61, S60–S70.

Bonfante, B., Faux, P., Navarro, N., Mendoza-Revilla, J., Dubied, M., Montillot, C., Wentworth, E., Poloni, L., Varón-González, C., Jones, P., et al., 2021. A GWAS in

Latin Americans identifies novel face shape loci, implicating VPS13B and a Denisovan introgressed region in facial variation. Sci. Adv. 7, eabc6160.
Bult, C.J., Blake, J.A., Smith, C.L., Kadin, J.A., Richardson, J.E., Anagnostopoulos, A., Asabor, R., Baldarelli, R.M., Beal, J.S., Bello, S.M., et al., 2019. Mouse Genome Database (MGD) 2019. Nucleic Acids Res. 47, D801–D806.
Bulut, O., Gungor, K., Thiemann, N., Hizliol, I., Gurcan, S., Hekimoglu, B., Kaya, E., Ozdede, M., Akay, G., 2017. Repeatability of facial soft tissue thickness measurements for forensic facial reconstruction using X-ray images. Aust. J. Forensic Sci. 49, 134–141.
Calloni, G.W., Le Douarin, N.M., Dupin, E., 2009. High frequency of cephalic neural crest cells shows coexistence of neurogenic, melanogenic, and osteogenic differentiation capacities. Proc. Natl. Acad. Sci. U. S. A. 106, 8947–8952.
Cha, S., Lim, J.E., Park, A.Y., Do, J.H., Lee, S.W., Shin, C., Cho, N.H., Kang, J.O., Nam, J.M., Kim, J.S., et al., 2018. Identification of five novel genetic loci related to facial morphology by genome-wide association studies. BMC Genomics 19, 481.
Chen, G., Xu, H., Yao, Y., Xu, T., Yuan, M., Zhang, X., Lv, Z., Wu, M., 2020. BMP signaling in the development and regeneration of cranium bones and maintenance of calvarial stem cells. Front. Cell Dev. Biol. 8, 135.
Chen, Y., Branicki, W., Walsh, S., Nothnagel, M., Kayser, M., Liu, F., Consortium, V., 2021. The impact of correlations between pigmentation phenotypes and underlying genotypes on genetic prediction of pigmentation traits. Forensic Sci. Int. Genet. 50, 102395.
Claes, P., Liberton, D.K., Daniels, K., Rosana, K.M., Quillen, E.E., Pearson, L.N., McEvoy, B., Bauchet, M., Zaidi, A.A., Yao, W., et al., 2014. Modeling 3D facial shape from DNA. PLoS Genet. 10, e1004224.
Claes, P., Roosenboom, J., White, J.D., Swigut, T., Sero, D., Li, J., Lee, M.K., Zaidi, A., Mattern, B.C., Liebowitz, C., et al., 2018. Genome-wide mapping of global-to-local genetic effects on human facial shape. Nat. Genet. 50, 414–423.
Cole, J.B., Manyama, M., Kimwaga, E., Mathayo, J., Larson, J.R., Liberton, D.K., Lukowiak, K., Ferrara, T.M., Riccardi, S.L., Li, M., et al., 2016. Genomewide association study of African children identifies association of SCHIP1 and PDE8A with facial size and shape. PLoS Genet. 12, e1006174.
Cole, J.B., Manyama, M., Larson, J.R., Liberton, D.K., Ferrara, T.M., Riccardi, S.L., Li, M., Mio, W., Klein, O.D., Santorico, S.A., et al., 2017. Human facial shape and size heritability and genetic correlations. Genetics 205, 967–978.
Crouch, D.J.M., Winney, B., Koppen, W.P., Christmas, W.J., Hutnik, K., Day, T., Meena, D., Boumertit, A., Hysi, P., Nessa, A., et al., 2018. Genetics of the human face: identification of large-effect single gene variants. Proc. Natl. Acad. Sci. U. S. A. 115, E676–E685.
De Greef, S., Claes, P., Vandermeulen, D., Mollemans, W., Suetens, P., Willems, G., 2006. Large-scale in-vivo Caucasian facial soft tissue thickness database for craniofacial reconstruction. Forensic Sci. Int. 159, S126–S146.
Delaneau, O., Marchini, J., Zagury, J.F., 2011. A linear complexity phasing method for thousands of genomes. Nat. Methods 9, 179–181.
Dryden, I.L., Mardia, K.V., 2016. Statistical shape analysis with applications in R, second ed. Wiley, Chichester, UK.
Duan, F.Q., Yang, Y.C., Li, Y., Tian, Y., Lu, K., Wu, Z.K., Zhou, M.Q., 2014. Skull identification via correlation measure between skull and face shape. IEEE Trans. Inf. Forensics Secur. 9, 1322–1332.
Elouej, S., Harhouri, K., Le Mao, M., Baujat, G., Nampoothiri, S., Kayserili, H., Al Menabawy, N., Selim, L., Paneque, A.L., Kubisch, C., et al., 2020. Loss of MTX2 causes mandibuloacral dysplasia and links mitochondrial dysfunction to altered nuclear morphology. Nat. Commun. 11, 4589.
Genomes Project, C., Auton, A., Brooks, L.D., Durbin, R.M., Garrison, E.P., Kang, H.M., Korbel, J.O., Marchini, J.L., McCarthy, S., McVean, G.A., et al., 2015. A global reference for human genetic variation. Nature 526, 68–74.
Gottesman, I.I., Gould, T.D., 2003. The endophenotype concept in psychiatry: etymology and strategic intentions. Am. J. Psychiatry 160, 636–645.
Greenwood, T.A., Lazzeroni, L.C., Maihofer, A.X., Swerdlow, N.R., Calkins, M.E., Freedman, R., Green, M.F., Light, G.A., Nievergelt, C.M., Nuechterlein, K.H., et al., 2019. Genome-wide association of endophenotypes for schizophrenia from the Consortium on the Genetics of Schizophrenia (COGS) study. JAMA Psychiatry 76, 1274–1284.
Howie, B.N., Donnelly, P., Marchini, J., 2009. A flexible and accurate genotype imputation method for the next generation of genome-wide association studies. PLoS Genet. 5, e1000529.
Huang, Y., Li, D., Qiao, L., Liu, Y., Peng, Q., Wu, S., Zhang, M., Yang, Y., Tan, J., Xu, S., et al., 2020. A genome-wide association study of facial morphology identifies novel genetic loci in Han Chinese. J. Genet. Genomics 48, 198–207.
Hwang, H.S., Choe, S.Y., Hwang, J.S., Moon, D.N., Hou, Y., Lee, W.J., Wilkinson, C., 2015. Reproducibility of facial soft tissue thickness measurements using cone-beam CT images according to the measurement methods. J. Forensic Sci. 60, 957–965.
Kim, S.H., Shin, H.S., 2018. Three-dimensional analysis of the correlation between soft tissue and bone of the lower face using three-dimensional facial laser scan. J. Craniofac. Surg. 29, 2048–2054.
Lee, M.K., Shaffer, J.R., Leslie, E.J., Orlova, E., Carlson, J.C., Feingold, E., Marazita, M.L., Weinberg, S.M., 2017. Genome-wide association study of facial morphology reveals novel associations with FREM1 and PARK2. PLoS ONE 12, e0176566.
Li, J., Ji, L., 2005. Adjusting multiple testing in multilocus analyses using the eigenvalues of a correlation matrix. Heredity 95, 221–227.
Li, Y., Zhao, W., Li, D., Tao, X., Xiong, Z., Liu, J., Zhang, W., Ji, A., Tang, K., Liu, F., et al., 2019. *EDAR*, *LYPLAL1*, *PRDM16*, *PAX3*, *DKK1*, *TNFSF12*, *CACNA2D3*, and *SUPT3H* gene variants influence facial morphology in a Eurasian population. Hum. Genet. 138, 681–689.
Lippert, C., Sabatini, R., Maher, M.C., Kang, E.Y., Lee, S., Arikan, O., Harley, A., Bernal, A., Garst, P., Lavrenko, V., et al., 2017. Identification of individuals by trait prediction using whole-genome sequencing data. Proc. Natl. Acad. Sci. U. S. A. 114, E8800.
Liu, F., van der Lijn, F., Schurmann, C., Zhu, G., Chakravarty, M.M., Hysi, P.G., Wollstein, A., Lao, O., de Bruijne, M., Ikram, M.A., et al., 2012. A genome-wide association study identifies five loci influencing facial morphology in Europeans. PLoS Genet. 8, e1002932.
Massey, F.J., 1951. The Kolmogorov-Smirnov test for goodness of fit. J. Am. Stat. Assoc. 46, 68–78.
Miller, G.A., Rockstroh, B.S., 2016. Progress and prospects for endophenotypes for schizophrenia in the time of genomics, epigenetics, oscillatory brain dynamics, and the research domain criteria, in: Abel, T., Nickl-Jockschat, T. (Eds.), The Neurobiology of Schizophrenia. Academic Press, San Diego, pp. 17–38.
Montufar, J., Romero, M., Scougall-Vilchis, R.J., 2018. Automatic 3-dimensional cephalometric landmarking based on active shape models in related projections. Am. J. Orthod. Dentofacial Orthop. 153, 449–458.
Paternoster, L., Zhurov, A.I., Toma, A.M., Kemp, J.P., St Pourcain, B., Timpson, N.J., McMahon, G., McArdle, W., Ring, S.M., Smith, G.D., et al., 2012. Genome-wide association study of three-dimensional facial morphology identifies a variant in PAX3 associated with nasion position. Am. J. Hum. Genet. 90, 478–485.
Pickrell, J.K., Berisa, T., Liu, J.Z., Ségurel, L., Tung, J.Y., Hinds, D.A., 2016. Detection and interpretation of shared genetic influences on 42 human traits. Nat. Genet. 48, 709–717.
Preston, G.A., Weinberger, D.R., 2005. Intermediate phenotypes in schizophrenia: a selective review. Dialogues Clin. Neurosci. 7, 165–179.
Qiao, L., Yang, Y., Fu, P., Hu, S., Zhou, H., Peng, S., Tan, J., Lu, Y., Lou, H., Lu, D., et al., 2018. Genome-wide variants of Eurasian facial shape differentiation and a prospective model of DNA based face prediction. J. Genet. Genomics 45, 419–432.
Seselj, M., Duren, D.L., Sherwood, R.J., 2015. Heritability of the human craniofacial complex. Anat. Rec. 298, 1535–1547.
Shaffer, J.R., Orlova, E., Lee, M.K., Leslie, E.J., Raffensperger, Z.D., Heike, C.L., Cunningham, M.L., Hecht, J.T., Kau, C.H., Nidey, N.L., et al., 2016. Genome-wide association study reveals multiple loci influencing normal human facial morphology. PLoS Genet. 12, e1006149.
Shannon, P., Markiel, A., Ozier, O., Baliga, N.S., Wang, J.T., Ramage, D., Amin, N., Schwikowski, B., Ideker, T., 2003. Cytoscape: a software environment for integrated models of biomolecular interaction networks. Genome Res. 13, 2498–2504.
Simmons-Ehrhardt, T., Falsetti, C., Falsetti, A.B., Ehrhardt, C.J., 2018. Open-source tools for dense facial tissue depth mapping of computed tomography models. Hum. Biol. 90, 63–76.
Simpson, E., Henneberg, M., 2002. Variation in soft-tissue thicknesses on the human face and their relation to craniometric dimensions. Am. J. Phys. Anthropol. 118, 121–133.
Stephan, C.N., Simpson, E.K., 2008. Facial soft tissue depths in craniofacial identification (part I): an analytical review of the published adult data. J. Forensic Sci. 53, 1257–1272.
Szklarczyk, D., Gable, A.L., Lyon, D., Junge, A., Wyder, S., Huerta-Cepas, J., Simonovic, M., Doncheva, N.T., Morris, J.H., Bork, P., et al., 2019. STRING v11: protein-protein association networks with increased coverage, supporting functional discovery in genome-wide experimental datasets. Nucleic Acids Res. 47, D607–D613.
Tsagkrasoulis, D., Hysi, P., Spector, T., Montana, G., 2017. Heritability maps of human face morphology through large-scale automated three-dimensional phenotyping. Sci. Rep. 7, 45885.
Weinberg, S.M., Parsons, T.E., Marazita, M.L., Maher, B.S., 2013. Heritability of face shape in twins: a preliminary study using 3D stereophotogrammetry and geometric morphometrics. Dent. 3000 1, 14.
White, J.D., Indencleef, K., Naqvi, S., Eller, R.J., Hoskens, H., Roosenboom, J., Lee, M.K., Li, J., Mohammed, J., Richmond, S., et al., 2021. Insights into the genetic architecture of the human face. Nat. Genet. 53, 45–53.
Wu, W., Zhai, G., Xu, Z., Hou, B., Liu, D., Liu, T., Liu, W., Ren, F., 2019. Whole-exome sequencing identified four loci influencing craniofacial morphology in northern Han Chinese. Hum. Genet. 138, 601–611.
Xiong, Z., Dankova, G., Howe, L.J., Lee, M.K., Hysi, P.G., de Jong, M.A., Zhu, G., Adhikari, K., Li, D., Li, Y., et al., 2019. Novel genetic loci affecting facial shape variation in humans. Elife 8, e49898.
Yun, H.S., Jang, T.J., Lee, S.M., Lee, S.H., Seo, J.K., 2020. Learning-based local-to-global landmark annotation for automatic 3D cephalometry. Phys. Med. Biol. 65, 0850.
Zakany, J., Kmita, M., Duboule, D., 2004. A dual role for *Hox* genes in limb anterior-posterior asymmetry. Science 304, 1669–1672.
Zhou, Y., Zhou, B., Pache, L., Chang, M., Khodabakhshi, A.H., Tanaseichuk, O., Benner, C., Chanda, S.K., 2019. Metascape provides a biologist-oriented resource for the analysis of systems-level datasets. Nat. Commun. 10, 1523.
Zhuang, X., Arridge, S., Hawkes, D.J., Ourselin, S., 2011. A nonrigid registration framework using spatially encoded mutual information and free-form deformations. IEEE Trans. Med. Imaging 30, 1819–1828.